ADAPTIVE THIRD-ORDER VOLTERRA FILTER FOR DETECTION AND TRACKING OF NONLINEAR OSCILLATIONS IN ULTRASOUND ECHO DATA

*Juan Du, John R. Ballard, Jeunghwan Choi, John C. Bischof and Emad S. Ebbini**

University of Minnesota
College of Science and Engineering
Minneapolis, MN 55455
{duxxx134, ball0250, choi0158, bischof, emad}@umn.edu

ABSTRACT

Microbubble ultrasound contrast agents (UCAs) have been extensively used in medical ultrasound for enhancing the echo components from blood vessels. However, their ultimate promise of enhancing the echoes from the microvasculature with high specificity remains unfulfilled using existing methods. We have previously shown that the Volterra filter can be used to enhance UCA echo components from flow channels with dimensions similar to peripheral vessels, e.g. the carotid artery. In this paper, we investigate a new receiver architecture based on an adaptive third-order Volterra Filter (VF) in conjunction with beamformed echo data from imaging tumor microvasculature *in vivo*. It is shown that the cubic and quadratic components of the VF provide significant enhancement of the UCA echoes from the tumor compared to the echoes from the same tissue regions in the absence of the UCA. We describe an adaptive recursive least squares (RLS) implementation of the VF and give examples of the contrast enhancement. Further enhancement of the UCA contrast is achieved by applying a dynamic statistical decision rule that produces a parameter we refer to as the temporal perfusion index (TPI). The TPI rewards transient echo oscillations while rejecting tissue motion and noise variation. These *in vivo* results demonstrate the potential for advanced signal processing in increasing the sensitivity and specificity of medical ultrasound in imaging tissue perfusion, a form of functional imaging.

Index Terms— Nonlinear Signal Processing, Ultrasound Imaging, Functional Imaging, Postbeamforming Filter Banks

1. INTRODUCTION

Microbubble ultrasound contrast agents (UCAs) are increasingly being used for both diagnostic and therapeutic purposes in medical ultrasound. The majority of UCAs in use today are gas-filled thin shells 1 - 5 μm in diameter, with the shell material and construction carefully selected and designed to produce nonlinear echo oscillations when excited by the transmit imaging beam. These oscillations mix with the (largely) linear tissue response and appear at the output of the receive beamformed echo signal. In well perfused organs such as the heart, the UCA echoes are prominent even in the standard imaging mode, the so-called B-mode on clinical ultrasound scanners. In poorly vascularized tissues such as necrotic tumors and diseased tissues, however, UCA echo oscillations are at or slightly above the noise level and cannot be observed in B-mode images. Post-beamforming signal processing methods have been investigated for enhancement of nonlinear echo oscillations due to UCA and suppression of tissue components with the most notable being the pulse inversion method [1]. Harmonic B mode imaging seeks to remove the fundamental frequency to improve the imaging of the harmonics at the cost of lowered imaging resolution [2]. On the other hand, pulse inversion overcomes the trade off between contrast and spatial resolution, but it is sensitive to tissue motion [3].

We have previously introduced the post-beamforming VF as an efficient method for separating linear and quadratic and cubic components in pulse-echo ultrasound. The main advantages of this filter are the improved dynamic range of the data and the rejection of additive Gaussian noise. Compared with the pulse inversion method, the VF offers the advantage of improved noise rejection by virtue of its rejection of additive Gaussian noise. In addition, the VF is capable of extracting noise components that reside within the signal bandwidth, i.e. not a harmonic filter. We have demonstrated these advantages in tissue mimicking flow phantoms with flow channel dimensions of similar size to peripheral vessels such as the carotid artery. However, the ultimate goal (and challenge) in UCA imaging is detection and separation of extremely small nonlinear echo components from microvessels. This allows the use of ultrasound to image blood perfusion in tissue, which is most valuable in the assessment of the health of the tissue, e.g. imaging necrotic tumors, ischemic tissue, etc. To the best of our knowledge, there has been no demonstration

*Funded in part by a grant from the Office of Vice President for Research, University of Minnesota.

of this imaging capability at frequencies suitable for clinical use.

Our previous studies employed a minimum-norm least squares (MNLS) algorithm for estimating the VF coefficient using segments of echo data from selected tissue locations representative of the UCA activity [4]. In this paper, we use an adaptive RLS approach for estimating the VF filter coefficient and it is shown to provide significant improvement in the UCA contrast enhancement. The results, using data from *in vivo* imaging of tumors with heterogeneous blood perfusion, demonstrate the ability of the VF approach to enhance UCA contrast in low echogenicity tissue. Furthermore, we also demonstrate the use of a post-VF dynamic statistical decision rule for the detection and characterization of tissue perfusion. This temporal perfusion index (TPI) produces significant enhancement of UCA echoes which makes easier to visualize perfusion images fused with anatomical imaging data. It also has the potential to quantify perfusion for clinical applications.

2. METHODS

We describe the postbeamforming signal processing of echo data from a clinical ultrasound scanner where the data samples are available in raw RF (radio frequency) form. As such the data is similar to sampled data from a communication channel, i.e. with a carrier frequency, f_0, and finite bandwidth, B, such that the $f_0 - B >> 0$.

2.1. *In Vivo* Imaging and Data Collection

Contrast enhanced ultrasound imaging was done on dunning AT-1 prostate cancer tumor embedded in the hind limb of a Copenhagen rat. The rats were anesthetized with Ketamine and Xylazine and placed in a supine position. The imaging data was collected with a linear diagnostic array probe (HST 15-8, Ultrasonix, Richmond, BC Canada) connected to a Sonix RP commercial ultrasound scanner with a research interface (Ultrasonix). Images were obtained before and after injection of .75 mL of MicroMarker UCA (Visual Sonics, Toronto, ON Canada). Beamformed rf data was collected at 40 MHz sampling frequency and stored for offline processing.

2.2. Postbeamforming VF Implementation

The Volterra filter is a nonlinear filter with memory that has been used widely in the signal and imaging processing community to separate linear and nonlinear signals [5]. For a 3rd order VF, the input output equation is given by:

$$\begin{aligned} x[n+1] &= \sum_{i=0}^{m-1} x[n-i]h_L[i] \\ &+ \sum_{i=0}^{m-1}\sum_{j=0}^{m-1} x[n-i]x[n-j]h_Q[i,j] \\ &+ \sum_{i=0}^{m-1}\sum_{j=0}^{m-1}\sum_{k=0}^{m-1} x[n-i]x[n-j]x[n-k]h_C[i,j,k] \end{aligned} \quad (1)$$

where $x[n]$ is beamformer output, m is the system order, and $h_L[n], h_Q[n], h_C[n]$ are the coefficients of the linear, quadratic and cubic filter, respectively.

While nonlinear in $x[n]$, (1) is linear in the filter coefficients. Taking the coefficient symmetry into account, (1) can be written in compact vector form:

$$\begin{aligned} X[n] =& [x[n], x[n-1], ..., x[n-m+1], \\ & x^2[n], x[n]*x[n-1], ..., x^2[n-m+1], \\ & x^3[n], x^2[x]*x[n-1], ..., x^3[n-m+1]]^T; \\ H[n] =& [h_L[0], h_L[1], ..., h_L[m-1], \\ & h_Q[0,0], h_Q[0,1], ..., h_Q[m-1,m-1], \\ & h_C[0,0,0], ..., h_C[m-1,m-1,m-1]]^T; \\ x[n+1] =& H^T[n]X[n]; \end{aligned} \quad (2)$$

with the data and coefficient vectors as defined. This equation can be written for M values of n, which leads to a system of linear equation that can be solved using the pseudoinverse (MNLS solution [1]).

2.3. Adaptive RLS Algorithm

The advantages of RLS adaptive filter formulation are well established for the linear case and they continue to hold in the VF case. In general, the RLS algorithm achieves fast convergence while producing small steady-values of the ensemble-average squared error [6]. In this paper, the following adaptive RLS algorithm was used:

$$\begin{aligned} k[n] &= \frac{P[n-1]X[n]}{\lambda + X^H[n]P[n-1]X[n]]}, \\ \xi[n] &= x[n+1] - H^H[n-1]X[n], \\ H[n] &= H[n-1] + k[n]\xi^*[n], \\ P[n] &= \lambda^{-1}(P[n-1] - k[n]X^H[n]P[n-1]) \end{aligned} \quad (3)$$

where $\xi[n]$, $P[n]$ and $k[n]$ are the prior estimate error. the inverse of the correlation matrix, and the Kalman gain vector, respectively.

2.4. Temporal Perfusion Index

The use of the VF improved dynamic range and SNR at the output of the VF, in addition to its higher sensitivity to nonlinear oscillations, improves the detection of the UCA, especially in low echogenicity regions. However, it is possible to achieve further enhancement of the UCA oscillations by employing a dynamic decision rule or metric that rewards the variance of the echo strength over finite horizon. This is due to the fact that the echogenicity of microbubbles in low perfusion, low echogenicity tissue is a transient event, i.e. oscillations appear and disappear with the incoming and outgoing microbubbles. One such metric is the TPI metric [7], which seeks to find the locations where the signal varies transiently

over time, and thus can be assumed to be representative of microvasculature. The equation for TPI is defined by

$$TPI(x,z,t) = \frac{var\left\{I(x,z,t)\right\}}{mean^2\left\{I(x,z,t)\right\}}, t \in [t_0 - T, t_0], \quad (4)$$

where, x and z are the lateral and axial coordinates of the pixel, and t_0 is the time (frame) index. T is appropriately selected based on the subjects' motion (breathing, heart cycle, etc...) and effectively be chosen to correspond to one respiratory cycle. The TPI metric is applied on the filtered log-compressed imaging data of each component acquired from the output of the TVF.

Variance is sensitive to the movement. In order to enhance the perfusion movement, especially the small echoes, mean square is needed to normalize the result. Therefore, TPI is a good way to display microbubble movement while distinguishing perfusion from stationary or even small movement tissues.

3. RESULTS AND DISCUSSION

The adaptive RLS algorithm described above was run using $m = 15$ to find the kernel coefficients. The algorithm proved to be superior to the MNLS approach in terms of minimizing the prediction error and its convergence was fast as expected. Specifically, convergence was achieved in 173 steps (samples) using an echo segment from a high echogenicity region at tumor-tissue boundary. The MNLS VF appeared to consistently overestimate the high frequency signal components sometimes exceeding the energy observed at the beamformer output. Therefore, we only show the results from the adaptive RLS VF as a preferred implementation from both the performance and feasibility stand points.

3.1. Spectral Analysis of Adaptive VF Outputs

Analysis of the spectral characteristics of the VF output components with and without UCA oscillations sheds light on the potential for contrast enhancement. Figure 1 (top) shows the PSD of the linear, quadratic, and cubic components of the adaptive RLS VF using data segments from the tumor region with and without contrast. Note that the linear components represent the corresponding beamformer output components (input to the VF) and are not shown to save space. The outputs from the linear, quadratic, and cubic components are consistent with our previous observations using the second-order and third-order VF with pulse-echo ultrasound, e.g. quadratic components with peaks near DC and near the 2nd harmonic, cubic components near the fundamental and 3rd harmonic). More importantly, the sensitivity to the presence of UCA is evident throughout the spectrum. One can also observe that a higher relative UCA enhancement can be expected using the cubic component compared to the quadratic component. The latter, in turn, has the potential of improving enhancement compared to the linear component.

Figure 1 (bottom) shows the PSDs obtained from the three adaptive RLS output components obtained when the input RF data were from a high echogenicity tissue region. While the spectra show some sensitivity to the presence of contrast in this case, the differences indicate that the potential for discrimination is diminished compared to the low echogenicity case described above. The nonlinear components are relatively higher in this case, with and without UCA, indicating that the beamformed data has significant nonlinear component due to propagation.

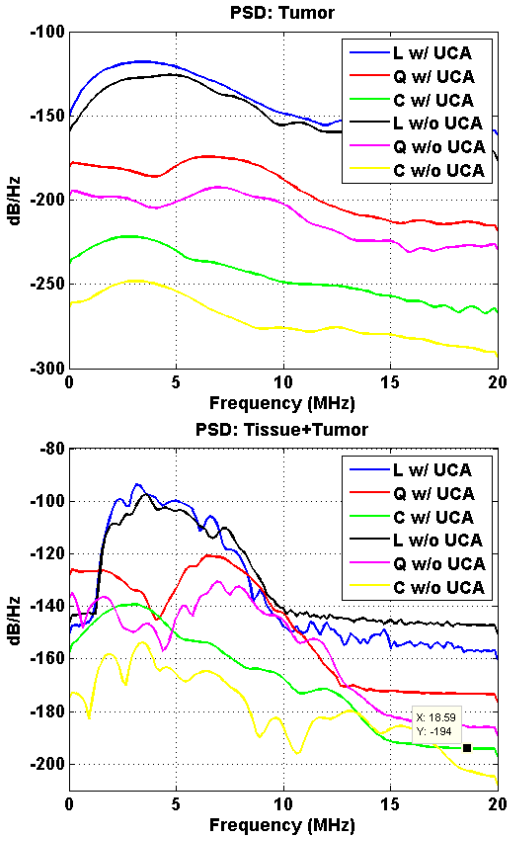

Fig. 1. PSDs of post-beamforming signal components (linear, quadratic, and cubic) from representative tumor echoes (top) and representative tissue+ tumor echoes (bottom).

3.2. Statistical Distribution of VF Output Components

The statistical distribution of the filter outputs enlightens the design of subsequent steps in the receiver signal processing chain. Figure 2 shows histograms of log-compressed outputs from the VF filter components with and without contrast agents. The top panel shows histograms from 72 image lines passing through the tumor while the bottom panel shows the histograms from the whole frame data.

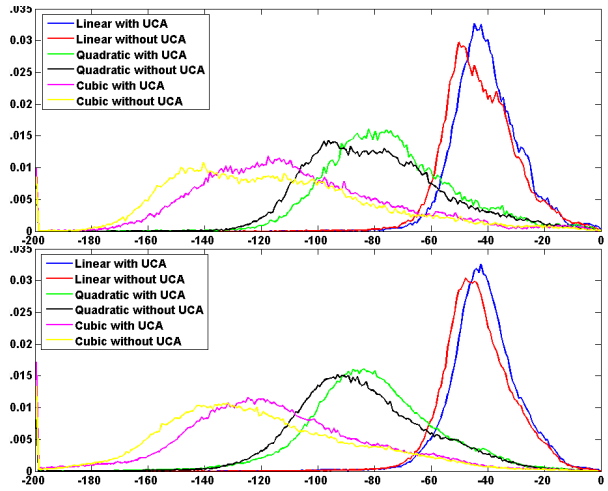

Fig. 2. Histograms of the output components of the VF with and without contrast: Top: Tissue+Tumor from beamformed image lines passing through the tumor. Bottom: Data from the whole image frame.

Both sets of histograms show that all three components of the VF output have sensitivity to UCA as demonstrated by the increase in the mean. However, the histograms in the top figure are more likely to separate the UCA and tissue components. In addition, they appear to be multimodal while the histograms generated from the whole frame appear to be unimodal Fisher-Tippet distribution. In this paper, we simply used these histograms to define thresholds for the dynamic range of each image component for the purpose of computing the TPI.

3.3. Temporal Perfusion Index

Based on the spectral representation and the histograms shown above, we have computed the TPI using the cubic component of the adaptive VF output after limiting the dynamic range to 120 dB. To illustrate the value of the TPI, we show a spatial temporal representation of this quantity along one image line passing through the tumor with and without UCA. The false color images in Figure 3 show a spatial-temporal representation of the TPI for one image line passing through the tumor without (top) and with (bottom) UCA. One can see the drastic difference in visibility of transient components within the tumor boundaries when the UCA is present.

4. CONCLUSION

This paper presented the first full demonstration of the capabilities of the VF, when implemented in adaptive RLS filter form, to detect the minute changes in echogenicity due to nonlinear oscillations generated by UCA microbubbles under

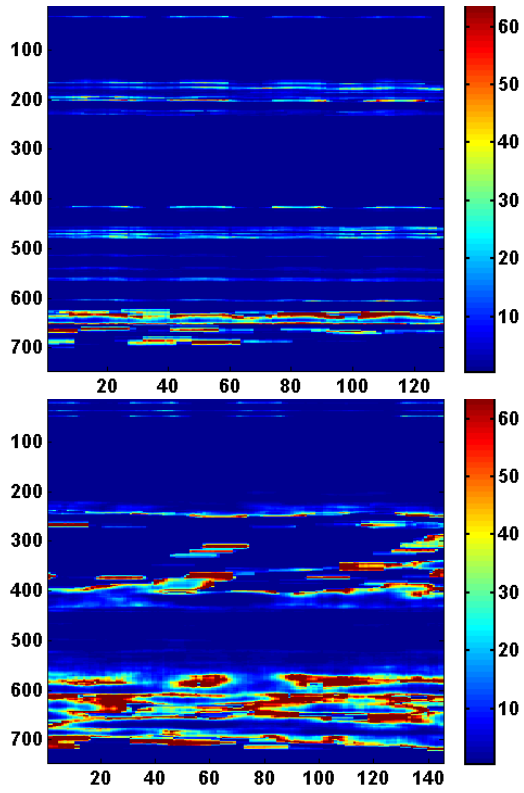

Fig. 3. Spatial-temporal representation of TPI along one image line passing through the tumor. Labeling in pixels axially and in frame number laterally. The tumor segment extends from 200 – 450 axially. Top: TPI without UCA. Bottom: TPI with UCA.

the influence of diagnostic imaging beams. Compared to the raw RF data, the quadratic and cubic outputs of the adaptive RLS VF exhibit higher sensitivity to the presence of UCA oscillations in tumor and normal tissues. In this paper, we have used the adaptive RLS VF to process *In vivo* echo data from a poorly vascularized tumor implanted in a small animal, which is highly relevant for current research and future clinical applications. These result highlight the role of signal processing in moving medical ultrasound imaging to provide more quantitative and/or functional imaging, which is the future of all medical imaging.

Relationship to Prior Work: To the best of our knowledge, this paper presents the first exposition of the spectral and statistical characteristics of the linear and nonlinear VF outputs resulting from echo data generated by a normal and tumor tissues *in vivo*. Compared to our previous work [4], we have established the adaptive RLS implementation as the method of choice not only from the error minimization viewpoint, but also from a practical implementation one. We are currently investigating the regional statistics of ultrasound images in tumor and healthy tissue and their implication on the design of perfusion measures such as the TPI.

5. REFERENCES

[1] Pornchai Phukpattaranont and Emad S. Ebbini, "Post-beamforming second-order volterra filter for pulse-echo ultrasonic imaging," *IEEE Transactions on Ultrasonics, Ferroelectrics, and Frequency Control*, vol. 50, pp. 987–1001, Aug. 2003.

[2] D.H. Simpson, Chien Ting Chin, and P.N. Burns, "Pulse inversion doppler: A new method for detecting nonlinear echoes from microbubble contrast agents," *IEEE Transactions on Ultrasonics, Ferroelectrics, and Frequency Control*, vol. 46, pp. 372–382, Mar. 1999.

[3] Che-Chou Shen and Pai-Chi Li, "Motion artifacts of pulse inversion-based tissue harmonic imaging," *IEEE Transactions on Ultrasonics, Ferroelectrics, and Frequency Control*, vol. 49, pp. 1203–1211, Sep. 2002.

[4] M.F. Al-Mistarihi, P. Phukpattaranont, and E.S. Ebbini, "Post-beamforming third-order volterra filter (thovf) for pulse-echo ultrasonic imaging," in *Acoustics, Speech and Signal Processing*. IEEE, 2004, vol. 3, pp. iii–97–100.

[5] V.J. Mathews, "Adaptive polynomial filters," *Signal Processing Magazine, IEEE*, vol. 8, pp. 10–26, Jul. 1991.

[6] Simon O. Haykin, *Adaptive Filter Theory*, Prentice Hall, fourth edition, 2001.

[7] Yayun Wan, Rachana Visaria, John C. Bischof, and Emad S. Ebbini, "Quadratic b-mode and pulse inversion imaging of perfusion defects in vivo," in *Life Science Systems and Applications Workshop*. IEEE/NIH, 2007, pp. 237–240.